

# Phenomenology of Two-Texture Zero Neutrino Mass Matrices

S. Dev<sup>\*</sup>, Sanjeev Kumar<sup>†</sup>, Surender Verma<sup>‡</sup> and Shivani Gupta<sup>§</sup>

Department of Physics, Himachal Pradesh University, Shimla 171005,  
INDIA

## Abstract

The generic predictions of two-texture zero neutrino mass matrices in the flavor basis have been examined especially in relation to the degeneracies between mass matrices within a class and interesting constraints on the neutrino parameters have been obtained. It is shown that the knowledge of the octant of  $\theta_{23}$ , the sign of  $\cos \delta$  and neutrino mass hierarchy can be used to lift these degeneracies.

## 1 Introduction

Mass matrices provide important tools for the investigation of the underlying symmetries and the resulting dynamics. The first step in this direction is the reconstruction of the neutrino mass matrix in the flavor basis. However, the reconstruction results in a large variety of possible structures of mass matrices depending strongly on the mass scale, mass hierarchy and the Majorana phases. However, the relatively weak dependence on some oscillation parameters ( $\theta_{23}$  and  $\delta$ ) results in the degeneracy of possible neutrino mass matrices. The mass matrix for Majorana neutrinos contains nine physical parameters including the three mass eigenvalues, three mixing angles and the three CP-violating phases. The two squared-mass differences ( $\Delta m_{12}^2$  and  $\Delta m_{13}^2$ ) and the two mixing angles ( $\theta_{12}$  and  $\theta_{23}$ ) have been measured in solar, atmospheric and reactor experiments. The third mixing angle  $\theta_{13}$  and the Dirac-type CP-violating phase  $\delta$  are expected to be measured in the forthcoming neutrino oscillation experiments. The possible measurement of the effective Majorana mass in neutrinoless double  $\beta$  decay searches will provide an additional constraint on the remaining three neutrino parameters viz. the neutrino mass scale and two Majorana-type CP-violating phases. While

---

<sup>\*</sup>dev5703@yahoo.com

<sup>†</sup>sanjeev3kumar@gmail.com

<sup>‡</sup>s\_7verma@yahoo.co.in

<sup>§</sup>shiroberts\_1980@yahoo.co.in

the neutrino mass scale will be independently determined by the direct beta decay searches and cosmological observations, the two Majorana phases will not be uniquely determined from the measurement of effective Majorana mass even if the absolute neutrino mass scale is known. Under the circumstances, it is natural to employ other theoretical inputs for the reconstruction of the neutrino mass matrix. The possible form of these additional theoretical inputs are limited by the existing neutrino data. Several proposals have been made in the literature to restrict the form of the neutrino mass matrix and to reduce the number of free parameters which include presence of texture zeros [1, 2, 3, 4, 5], requirement of zero determinant [6], the zero trace condition [7] to name just a few. However, the current neutrino oscillation data are consistent only with a limited number of texture schemes [1, 2, 3, 4, 5]. In particular, the current neutrino oscillation data disallow all neutrino mass matrices with three or more texture zeros in the flavor basis. Out of the fifteen possible neutrino mass matrices with two texture zeros, only seven are compatible with the current neutrino oscillation data. The seven allowed two texture zero mass matrices have been classified into three categories. The two class A matrices of the types  $A_1$  and  $A_2$  give normal hierarchy (NH) of neutrino masses. The class B matrices of types  $B_1$ ,  $B_2$ ,  $B_3$  and  $B_4$  yield a quasi-degenerate (QD) spectrum of neutrino masses. The single class C matrix corresponds to inverted hierarchy (IH) of neutrino masses.

In the absence of a significant breakthrough in the theoretical understanding of the fermion flavors, the phenomenological approaches are bound to play a crucial role in interpreting new experimental data on quark and lepton mixing. These approaches are expected to provide useful hints towards unraveling the dynamics of fermion mass generation, CP violation and identification of possible underlying symmetries of the lepton flavors from which realistic models of lepton mass generation and flavor mixing could be, hopefully, constructed.

Even though the grand unification on its own does not shed any light on the flavor problem, the Grand Unified Theories (GUTs) provide the optimal framework in which possible solutions to the flavor problem could be embedded. This is because the GUTs predict definite group theoretical relations between the fermion mass matrices. For this purpose, it is useful to find out possible leading order forms of the neutrino mass matrix in a basis in which the charged lepton mass matrix is diagonal. Such forms of neutrino mass matrix provide useful hints for model building which will eventually shed important light on the dynamics of lepton mass generation and flavor mixing. For example, a phenomenologically favored texture of quark mass matrix has been presented earlier [8]. In the spirit of quark-lepton similarity, the same texture has been prescribed for the charged lepton and Dirac neutrino mass matrices. The same texture for the right handed neutrino mass matrix in the see-saw mechanism might follow from universal flavor symmetry hidden in a more fundamental theory of mass generation. Thus, the texture zeros in different positions of the neutrino mass matrix, in particular and fermion mass matrices, in general could be consequence of an underlying symmetry [9, 10]. Such universal textures of fermion mass matrices can, theoretically, be obtained in the context of GUTs based on SO(10) [11]. Moreover, neutrino mass matrices with texture zeros have important implications for leptogenesis [12].

In the present work, we examine phenomenological implications of all possible neutrino mass matrices with two texture zeros. Neutrino mass matrices within a class were thought

to have identical phenomenological consequences [1, 2, 3] leading to degeneracy of mass matrices within a class. Thus, there is a two-fold degeneracy in class A while the neutrino mass matrices of class B exhibit an eight-fold degeneracy since normal/inverted hierarchies are practically indistinguishable because of quasi-degenerate spectrum of neutrino masses in this class. We study this degeneracy in detail and discuss possible ways to lift this degeneracy. It is found that the deviation of atmospheric mixing from maximality and the quadrant of the Dirac-type CP-violating phase  $\delta$  can be used to distinguish the mass matrices within a class. We, also, note that the determination of hierarchy will have important implications for class B neutrino mass matrices. The prospects for the measurement of  $\theta_{13}$  for class A neutrino mass matrices are quite optimistic since a definite lower bound on  $\theta_{13}$  is obtained for this class. For neutrino mass matrices of class B, CP-violation will be near maximal if  $\theta_{13}$  is large. Definite lower bounds on the effective Majorana mass  $M_{ee}$  are obtained for neutrino mass matrices of class B and C. Class D of neutrino mass matrices is disallowed in our analysis.

## 2 Neutrino mass matrix

The neutrino mass matrix,  $M$ , can be parameterized in terms of three neutrino mass eigenvalues ( $m_1, m_2, m_3$ ), three neutrino mixing angles ( $\theta_{12}, \theta_{23}, \theta_{13}$ ) and one Dirac-type CP violating phase,  $\delta$ . If neutrinos are Majorana particles then there are two additional CP violating phases  $\alpha, \beta$  in the neutrino mixing matrix. The complex symmetric mass matrix  $M$  can be diagonalized by a complex unitary matrix  $V$ :

$$M = V M_\nu^{diag} V^T \quad (1)$$

where  $M_\nu^{diag} = \text{Diag}\{m_1, m_2, m_3\}$ . The neutrino mixing matrix  $V$  [13] can be written as

$$V \equiv UP = \begin{pmatrix} c_{12}c_{13} & s_{12}c_{13} & s_{13}e^{-i\delta} \\ -s_{12}c_{23} - c_{12}s_{23}s_{13}e^{i\delta} & c_{12}c_{23} - s_{12}s_{23}s_{13}e^{i\delta} & s_{23}c_{13} \\ s_{12}s_{23} - c_{12}c_{23}s_{13}e^{i\delta} & -c_{12}s_{23} - s_{12}c_{23}s_{13}e^{i\delta} & c_{23}c_{13} \end{pmatrix} \begin{pmatrix} 1 & 0 & 0 \\ 0 & e^{i\alpha} & 0 \\ 0 & 0 & e^{i(\beta+\delta)} \end{pmatrix}, \quad (2)$$

where  $s_{ij} = \sin \theta_{ij}$  and  $c_{ij} = \cos \theta_{ij}$ . The matrix  $V$  is called the neutrino mixing matrix or PMNS matrix. The matrix  $U$  is the lepton analogue of the CKM quark mixing matrix and  $P$  contains the two Majorana phases.

The elements of the neutrino mass matrix can be calculated from Eq. (1). Some of the elements of  $M$ , which can be equated to zero in the various allowed texture zero schemes, are given by

$$M_{ee} = c_{13}^2 c_{12}^2 m_1 + c_{13}^2 s_{12}^2 m_2 e^{2i\alpha} + s_{13}^2 m_3 e^{2i\beta}, \quad (3)$$

$$M_{e\mu} = c_{13}\{s_{13}s_{23}e^{i\delta}(e^{2i\beta}m_3 - s_{12}^2e^{2i\alpha}m_2) - c_{12}c_{23}s_{12}(m_1 - e^{2i\alpha}m_2) - c_{12}^2s_{13}s_{23}e^{i\delta}m_1\}, \quad (4)$$

$$M_{e\tau} = c_{13}\{s_{13}c_{23}e^{i\delta}(e^{2i\beta}m_3 - s_{12}^2e^{2i\alpha}m_2) + c_{12}s_{23}s_{12}(m_1 - e^{2i\alpha}m_2) - c_{12}^2s_{13}c_{23}e^{i\delta}m_1\}, \quad (5)$$

$$M_{\mu\mu} = m_1(c_{23}s_{12} + e^{i\delta}c_{12}s_{13}s_{23})^2 + e^{2i\alpha}m_2(c_{12}c_{23} - e^{i\delta}s_{12}s_{13}s_{23})^2 + e^{2i(\beta+\delta)}m_3c_{13}^2s_{23}^2 \quad (6)$$

Type	Constraining Eqs.
$A_1$	$M_{ee} = 0, M_{e\mu} = 0$
$A_2$	$M_{ee} = 0, M_{e\tau} = 0$
$B_1$	$M_{e\tau} = 0, M_{\mu\mu} = 0$
$B_2$	$M_{e\mu} = 0, M_{\tau\tau} = 0$
$B_3$	$M_{e\mu} = 0, M_{\mu\mu} = 0$
$B_4$	$M_{e\tau} = 0, M_{\tau\tau} = 0$
$C$	$M_{\mu\mu} = 0, M_{\tau\tau} = 0$
$D_1$	$M_{\mu\mu} = 0, M_{\mu\tau} = 0$
$D_2$	$M_{\tau\tau} = 0, M_{\mu\tau} = 0$

Table 1: Allowed two texture zero mass matrices.

and

$$M_{\tau\tau} = m_1(s_{23}s_{12} - e^{i\delta}c_{12}s_{13}c_{23})^2 + e^{2i\alpha}m_2(c_{12}s_{23} + e^{i\delta}s_{12}s_{13}c_{23})^2 + e^{2i(\beta+\delta)}m_3c_{13}^2c_{23}^2. \quad (7)$$

It will be helpful to note from Eqs. (4-7) that the transformation

$$T \quad : \quad \theta_{23} \rightarrow \frac{\pi}{2} - \theta_{23}, \delta \rightarrow \delta + \pi \quad (8)$$

transforms  $M_{e\mu}$  to  $-M_{e\tau}$  and  $M_{\mu\mu}$  to  $M_{\tau\tau}$ . Therefore, if  $M_{e\mu}$  vanishes for  $\theta_{23}$  and  $\delta$ , then  $M_{e\tau}$  vanishes for  $\frac{\pi}{2} - \theta_{23}$  and  $\delta + \pi$ . Similarly, if  $M_{\mu\mu}$  vanishes for  $\theta_{23}$  and  $\delta$ , then  $M_{\tau\tau}$  vanishes for  $\frac{\pi}{2} - \theta_{23}$  and  $\delta + \pi$ . This fact can be, gainfully, used for distinguishing the subcategories of neutrino mass matrices within a class.

### 3 Two texture zeros

The neutrino mass matrix,  $M$ , in the charged lepton basis is given by Eq. (1). Out of the fifteen possible patterns for two texture zeros in  $M$ , the seven possibilities [1, 2], which are found to be consistent with the current neutrino oscillation data, are listed in Table 1. In addition, we have, also, included the two mass matrices of class D in the list. These mass matrices were disallowed in some of the earlier analyses [1, 2]. However, it was found in a subsequent detailed numerical analysis by Guo and Xing [3] that the neutrino mass matrices of class D are, marginally, allowed. The expressions for the vanishing elements in different two-zero texture schemes have been listed in Eqs. (4-7).

The transformation T defined in Eq. (8) transforms neutrino mass matrices of type  $A_1$  to  $A_2$  and neutrino mass matrices of type  $B_1$  ( $B_4$ ) to  $B_2$  ( $B_3$ ). Therefore, the predictions for neutrino mass matrices of types  $A_1$  and  $A_2$  will be identical for all neutrino parameters except  $\theta_{23}$  and/or  $\delta$ . Similarly, the predictions of neutrino mass matrices for all the four types of mass matrices in class B will be identical for all neutrino parameters except  $\theta_{23}$  and/or  $\delta$ . However, the different types of mass matrices will have different predictions for the octant of  $\theta_{23}$  and the sign of  $\cos \delta$ .

The two texture zeros in the neutrino mass matrix give two complex equations viz.

$$M_{ab} = 0, M_{pq} = 0 \quad (9)$$

where  $a, b, p$  and  $q$  can take values  $e, \mu$  and  $\tau$ . Eqs. (9) can, also, be written as

$$m_1 U_{a1} U_{b1} + m_2 U_{a2} U_{b2} e^{2i\alpha} + m_3 U_{a3} U_{b3} e^{2i(\beta+\delta)} = 0 \quad (10)$$

and

$$m_1 U_{p1} U_{q1} + m_2 U_{p2} U_{q2} e^{2i\alpha} + m_3 U_{p3} U_{q3} e^{2i(\beta+\delta)} = 0 \quad (11)$$

where  $U$  has been defined in Eq. (2). These two complex equations involve nine physical parameters  $m_1, m_2, m_3, \theta_{12}, \theta_{23}, \theta_{13}$  and CP-violating phases  $\alpha, \beta$ , and  $\delta$ . The two mixing angles  $(\theta_{12}, \theta_{23})$  and two mass-squared differences  $(\Delta m_{12}^2, \Delta m_{23}^2)$  are known from the solar, atmospheric and reactor neutrino experiments. The masses  $m_2$  and  $m_3$  can be calculated from the mass-squared differences  $\Delta m_{12}^2$  and  $\Delta m_{23}^2$  using the relations

$$m_2 = \sqrt{m_1^2 + \Delta m_{12}^2} \quad (12)$$

and

$$m_3 = \sqrt{m_2^2 + \Delta m_{23}^2}. \quad (13)$$

Thus, we have two complex relations relating five unknown parameters viz.  $m_1, \theta_{13}, \alpha, \beta$  and  $\delta$ . Therefore, if one out of these five parameters is assumed, other four parameters can be predicted. Thus, neutrino mass matrices with two texture zeros in the flavor basis have strong predictive power.

Solving Eqs. (10) and (11) simultaneously, we obtain

$$\frac{m_1}{m_3} e^{-2i\beta} = \frac{U_{p3} U_{q3} U_{a2} U_{b2} - U_{a3} U_{b3} U_{p2} U_{q2}}{U_{a1} U_{b1} U_{p2} U_{q2} - U_{a2} U_{b2} U_{p1} U_{q1}} e^{2i\delta} \quad (14)$$

and

$$\frac{m_1}{m_2} e^{-2i\alpha} = \frac{U_{p2} U_{q2} U_{a3} U_{b3} - U_{a2} U_{b2} U_{p3} U_{q3}}{U_{a1} U_{b1} U_{p3} U_{q3} - U_{a3} U_{b3} U_{p1} U_{q1}}. \quad (15)$$

Using Eqs. (14) and (15), the two mass ratios  $\left(\frac{m_1}{m_2}, \frac{m_1}{m_3}\right)$  and Majorana phases  $(\alpha, \beta)$  can be written as

$$\left(\frac{m_1}{m_2}\right) = \left| \frac{U_{p2} U_{q2} U_{a3} U_{b3} - U_{a2} U_{b2} U_{p3} U_{q3}}{U_{a1} U_{b1} U_{p3} U_{q3} - U_{a3} U_{b3} U_{p1} U_{q1}} \right|, \quad (16)$$

$$\left(\frac{m_1}{m_3}\right) = \left| \frac{U_{p3} U_{q3} U_{a2} U_{b2} - U_{a3} U_{b3} U_{p2} U_{q2}}{U_{a1} U_{b1} U_{p2} U_{q2} - U_{a2} U_{b2} U_{p1} U_{q1}} \right|, \quad (17)$$

$$\alpha = -\frac{1}{2} \arg \left( \frac{U_{p2} U_{q2} U_{a3} U_{b3} - U_{a2} U_{b2} U_{p3} U_{q3}}{U_{a1} U_{b1} U_{p3} U_{q3} - U_{a3} U_{b3} U_{p1} U_{q1}} \right) \quad (18)$$

and

$$\beta = -\frac{1}{2} \arg \left( \frac{U_{p3} U_{q3} U_{a2} U_{b2} - U_{a3} U_{b3} U_{p2} U_{q2}}{U_{a1} U_{b1} U_{p2} U_{q2} - U_{a2} U_{b2} U_{p1} U_{q1}} \right) - \delta. \quad (19)$$

Eqs. (18) and (19) give the Majorana phases  $\alpha$  and  $\beta$  in terms of  $\theta_{13}$  and  $\delta$  since  $\theta_{12}$  and  $\theta_{23}$  are known experimentally. Similarly, Eqs. (16) and (17) give the mass ratios  $\left(\frac{m_1}{m_2}, \frac{m_1}{m_3}\right)$  as functions of  $\theta_{13}$  and  $\delta$ . Since,  $\Delta m_{12}^2$  and  $\Delta m_{23}^2$  are known experimentally, the values of mass ratios  $\left(\frac{m_1}{m_2}, \frac{m_1}{m_3}\right)$  from Eqs. (16) and (17) can be used to calculate  $m_1$ . This can be done by inverting Eqs. (12) and (13) to obtain the two values of  $m_1$ , viz.

$$m_1 = \left(\frac{m_1}{m_2}\right) \sqrt{\frac{\Delta m_{12}^2}{1 - \left(\frac{m_1}{m_2}\right)^2}} \quad (20)$$

and

$$m_1 = \left(\frac{m_1}{m_3}\right) \sqrt{\frac{\Delta m_{12}^2 + \Delta m_{23}^2}{1 - \left(\frac{m_1}{m_3}\right)^2}}, \quad (21)$$

The two values of  $m_1$  obtained above from the mass ratios  $\left(\frac{m_1}{m_2}\right)$  and  $\left(\frac{m_1}{m_3}\right)$ , respectively, must be equal. Thus, we can constrain  $(\theta_{13}, \delta)$  plane using the experimental inputs for  $\Delta m_{12}^2$ ,  $\Delta m_{23}^2$ ,  $\theta_{12}$  and  $\theta_{23}$ . The Dirac-type CP violating phase,  $\delta$ , is given full variation from  $0^\circ$  to  $360^\circ$  and  $\theta_{13}$  is varied from zero to its upper bound from CHOOZ experiment. We use the current best fit values of the oscillation parameters with 1, 2 and 3  $\sigma$  [14] errors given below:

$$\begin{aligned} \Delta m_{12}^2 &= 7.9^{+0.3, 0.6, 1.0}_{-0.3, 0.6, 0.8} \times 10^{-5} \text{ eV}^2, \\ \Delta m_{23}^2 &= \pm 2.6^{+0.2, 0.4, 0.6}_{-0.2, 0.4, 0.6} \times 10^{-3} \text{ eV}^2, \\ s_{12}^2 &= 0.30^{+0.02, 0.06, 0.10}_{-0.02, 0.04, 0.06}, \\ s_{23}^2 &= 0.50^{+0.06, 0.13, 0.18}_{-0.05, 0.12, 0.16}, \\ s_{13}^2 &< 0.012, 0.025, 0.040. \end{aligned} \quad (22)$$

Here, '+' ('-') sign with the value of  $\Delta m_{23}^2$  is for normal (inverted) hierarchy. The analysis [14] incorporates not only the latest long baseline data for  $\Delta m_{13}^2$  from the MINOS collaboration [15] but also the updated KamLAND and SNO data [16]. We vary the oscillation parameters within their 1, 2 and 3  $\sigma$  C.L. ranges with uniform distributions and calculate their predictions at various confidence levels. However, we report the correlations plots at 1  $\sigma$  C.L.. We, also, calculate the Jarlskog rephasing invariant quantity [18]

$$J = s_{12}s_{23}s_{13}c_{12}c_{23}c_{13}^2 \sin \delta \quad (23)$$

for the allowed parameter space.

In our numerical analysis outlined above, the two squared-mass differences ( $\Delta m_{12}^2$  and  $\Delta m_{23}^2$ ) enter as two independent experimental inputs while the earlier analyses [1, 2, 3] require the ratio of two known mass-squared differences

$$R_\nu \equiv \frac{\Delta m_{12}^2}{\Delta m_{23}^2} = \frac{1 - \left(\frac{m_1}{m_2}\right)^2}{\left|1 - \frac{\left(\frac{m_1}{m_2}\right)^2}{\left(\frac{m_1}{m_3}\right)^2}\right|} \quad (24)$$

Type	$\frac{m_1}{m_2}$	$\frac{m_1}{m_3}$	$\alpha$	$\beta$
$A_1$	$\tan^2 \theta_{12}$	$\tan \theta_{12} \tan \theta_{23} \sin \theta_{13}$	$n + \frac{1}{2}\pi$	$\beta + \frac{\delta}{2} = n\pi$
$A_2$	$\tan^2 \theta_{12}$	$\frac{\tan \theta_{12} \sin \theta_{13}}{\tan \theta_{23}}$	$n + \frac{1}{2}\pi$	$\beta + \frac{\delta}{2} = (n + \frac{1}{2})\pi$
$B_1$	1	$\tan^2 \theta_{23}$	$n\pi$	$\beta + \delta = (n + \frac{1}{2})\pi$
$B_2$	1	$\frac{1}{\tan^2 \theta_{23}}$	$n\pi$	$\beta + \delta = (n + \frac{1}{2})\pi$
$B_3$	1	$\tan^2 \theta_{23}$	$n\pi$	$\beta + \delta = (n + \frac{1}{2})\pi$
$B_4$	1	$\frac{1}{\tan^2 \theta_{23}}$	$n\pi$	$\beta + \delta = (n + \frac{1}{2})\pi$
$C$	$\frac{1}{\tan^2 \theta_{12}}$	$\frac{1}{\tan \theta_{12} \tan 2\theta_{23} \sin \theta_{13}}$	$n + \frac{1}{2}\pi$	-
$D_1$	$\frac{1}{\tan^2 \theta_{12}}$	$\frac{\tan \theta_{23}}{\tan \theta_{12} \sin \theta_{13}}$	$n\pi$	$\beta + \frac{\delta}{2} = (n + \frac{1}{2})\pi$
$D_2$	$\frac{1}{\tan^2 \theta_{12}}$	$\frac{1}{\tan \theta_{23} \tan \theta_{12} \sin \theta_{13}}$	$n + \frac{1}{2}\pi$	$\beta + \frac{\delta}{2} = n\pi$

Table 2: Zeroth order approximations for neutrino mass matrices with two texture zeros.

to lie in the experimentally allowed range in order to constrain the other neutrino parameters. Our analysis makes direct use of the two mass-squared differences and has more constraining power whereas the earlier analyses which make use of the ratio  $R_\nu$  lose some of the constraining power because this procedure does not use the full experimental information currently available with us in the shape of two mass-squared differences. Moreover, since  $R_\nu$  is a function of mass ratios, it does not depend upon the absolute neutrino mass scale. It is obvious that the two mass ratios  $\left(\frac{m_1}{m_2}\right)$  and  $\left(\frac{m_1}{m_3}\right)$  may yield the experimentally allowed values of  $R_\nu$  [Eq. (24)] for mutually inconsistent values of  $m_1$  [Eqs. (20) and (21)]. Such mass ratios were allowed in the earlier analyses based upon  $R_\nu$  [1, 2, 3]. However, our analysis selects only those mass ratios for which the values of  $m_1$  obtained from Eqs. (20) and (21) are identical and the ratio  $R_\nu$  for these values of the mass ratios is automatically restricted to lie in the allowed experimental range. Moreover, the definition of  $R_\nu$

$$R_\nu \equiv \frac{\Delta m_{12}^2}{\Delta m_{23}^2} = \frac{|m_2^2 - m_1^2|}{|m_3^2 - m_2^2|} \quad (25)$$

used in many earlier analyses does not make use of the knowledge of solar mass hierarchy to constrain the neutrino parameter space. Our analysis disallows the class D of two-texture zero neutrino mass matrices which has been marginally allowed by Guo and Xing [3].

## 4 Results and discussion

In this section, we shall present the results of our numerical analysis for neutrino mass matrices of classes A, B and C based upon the approach described in the previous section. However, it will be helpful to know the Taylor series expansion of Eqs. (16-19) in the powers of  $s_{13}$  to appreciate the numerical results. The zeroth order terms of the Taylor series expansion have been tabulated in Table 2.

C.L.	$m_1(10^{-3}eV)$	$\alpha(\text{deg})$	$\beta(\text{deg})$	$\theta_{13}(\text{deg})$	$J$
1	2.6 - 4.5	83 - 97	-80 - 80	5.2 - 6.3	-0.025 - 0.025
2	2.1 - 8.9	77 - 103	-90 - 90	4.2 - 9.1	-0.037 - 0.037
3	1.7 - 13.4	73 - 107	-90 - 90	3.3 - 11.5	-0.046 - 0.046

Table 3: The predictions for neutrino mass matrices of class A.

1 $\sigma$ predictions	$\delta$	$\theta_{23}$
$A_1$	$-150^0 - 150^0$	$41.8^0 - 48.2^0$
$A_2$	$30^0 - 330^0$	$41.8^0 - 48.2^0$

Table 4: The predictions for  $\delta$  and  $\theta_{23}$  for neutrino mass matrices of types  $A_1$  and  $A_2$ .

## 4.1 Class A

It can be seen from Table 2 that both the mass ratios  $\frac{m_1}{m_2}, \frac{m_1}{m_3} \ll 1$  for neutrino mass matrices of class A. So, neutrino mass matrices of class A give hierarchical spectrum of neutrino masses. This case has, already, been analyzed analytically [5] and, here, we shall discuss the earlier results only for the sake of completeness.

The results for  $m_1$ ,  $\alpha$ ,  $\beta$ ,  $\theta_{13}$  and  $J$  for class A mass matrices have been summarized in Table 3 at various confidence levels. These quantities are the same for mass matrices of types  $A_1$  and  $A_2$ . It can be seen from Table 3 that the  $3\sigma$  lower bound on  $\theta_{13}$  is  $3.3^0$ . The range for the Majorana-type CP-violating phase  $\beta$  at  $1\sigma$  C.L. is found to be  $-80^0 - 80^0$ . However, if the neutrino oscillation parameters are allowed to vary beyond their present  $1.2\sigma$  C.L. ranges, the full range for  $\beta$  ( $-90^0 - 90^0$ ) is allowed. At one standard deviation, the allowed range of  $\delta$  is ( $-150^0 - 150^0$ ) for type  $A_1$  and ( $30^0 - 330^0$ ) for type  $A_2$  and the allowed range of  $\theta_{23}$  is ( $41.8^0 - 48.2^0$ ) for type  $A_1$  and  $A_2$  [Table 4]. Just like  $\beta$ , no constraint on  $\delta$  is obtained above  $1.2\sigma$  C.L. The accuracies of the oscillation parameters required to distinguish between the theoretical predictions of neutrino mass matrices of types  $A_1$  and  $A_2$  depend on the upper bound on  $\theta_{13}$ . With the current precision of the oscillation parameters, the neutrino mass matrices of types  $A_1$  and  $A_2$  can be distinguished at  $1\sigma$ ,  $2\sigma$  and  $3\sigma$  C.L. for  $\theta_{13} < 5.7^0, 5.2^0$  and  $4.8^0$  respectively.

Fig. 1 (identical for  $A_1$  and  $A_2$ ) depicts the correlation plots of  $m_1$ ,  $\alpha$ ,  $\beta$  and  $J$  at one standard deviation. Fig. 1(a) shows  $\alpha$  as a function of  $m_1$  and Fig1(b) shows  $\beta$  as a function of  $\alpha$ . The large spread in the  $(m_1, \alpha)$  plot is due to the errors in the neutrino oscillation parameters. However, there is a very strong correlation between  $\alpha$  and  $\beta$  as indicated in Table 2. Such a correlation between the Majorana phases was noted earlier [3]. However, full ranges ( $-90^0 - 90^0$ ) are allowed for the two Majorana phases in that analysis [3]. In contrast, we obtain a very narrow range for the Majorana phase  $\alpha$  around  $90^0$  [Cf. Table 3]. Similarly, the Majorana phase  $\beta$  is, also, constrained if the oscillation parameters are limited to their  $1\sigma$  ranges. Fig. 1(c) depicts the correlation between  $J$  and  $m_1$ .

In Fig. 2, we depict the correlation plots of  $\alpha$  and  $\beta$  with  $\delta$  for matrices of types  $A_1$  (left



panel) and  $A_2$  (right panel). We, also, show the correlation plots of  $\delta$  and  $\theta_{23}$  with one another as well as with  $\theta_{13}$  in Fig. 2. The Dirac-type CP-violating phase  $\delta$  is, strongly, correlated with the Majorana-type CP-violating phase  $\beta$  [Cf. Table 2]. It can be seen from  $(\alpha, \delta)$  correlation plots [Fig. 2(a) and 2(b)] and  $(\beta, \delta)$  correlation plots [Fig. 2(c) and 2(d)] that there are small deviations in the values of  $\alpha$  around  $90^\circ$  and the correlation between  $\beta$  and  $\delta$  is, almost, linear. The fact that  $\delta + 2\beta \simeq 0^\circ$  for  $A_1$  type mass matrices and  $\delta + 2\beta \simeq 180^\circ$  for  $A_2$  type mass matrices [cf. Table 2] is apparent from the  $(\beta, \delta)$  correlation plots [Fig. 2(c) and 2(d)]. The  $(\beta, \delta)$  correlation was noted earlier by Xing [2] in its approximate form in a different parameterization. The  $(\delta, \theta_{23})$  plots, clearly, illustrate the point that the neutrino mass matrices of types  $A_1$  and  $A_2$  prefer different regions on the  $(\delta, \theta_{23})$  plane. This is contrary to the analysis done by Xing [3] where no constraints on  $\delta$  and  $\theta_{23}$  have been obtained. In fact, this feature is crucial for distinguishing mass matrices of types  $A_1$  and  $A_2$  which were found to be degenerate in the earlier analyses [1, 2, 3]. The constraints on  $\delta$  and  $\theta_{23}$  are very sensitive to the values of  $\theta_{13}$ . For the values of  $\theta_{13}$  smaller than  $1\sigma$  CHOOZ bound, the constraints on  $\delta$  and  $\theta_{23}$  become stronger which can be seen from the  $(\theta_{13}, \theta_{23})$  and  $(\theta_{13}, \delta)$  correlation plots [Figures 2(g-j)]. For example, if  $\theta_{13} > 5.6^\circ$ , then  $\theta_{23} > 46^\circ$  (above maximal) for type  $A_1$  and  $\theta_{23} < 44^\circ$  (below maximal) for type  $A_2$ . It can, also, be seen from the  $(\theta_{13}, \theta_{23})$  correlation plots in Fig. 2 that the deviation of  $\theta_{23}$  from maximality is larger for smaller values of  $\theta_{13}$ . Therefore, if future experiments measure  $\theta_{13}$  below its present  $1\sigma$  bound, the neutrino mass matrices of types  $A_1$  and  $A_2$  will have different predictions for  $\delta$  and  $\theta_{23}$  with no overlap. However, it would be difficult to differentiate between matrices of types  $A_1$  and  $A_2$  if  $\theta_{13}$  is found to be above its present  $1\sigma$  range. As noted earlier, different quadrants for  $\delta$  are selected for neutrino mass matrices of types  $A_1$  and  $A_2$ . It can, also, be seen in Fig. 2 that the points  $\delta = 0, \pi$  are ruled out implying that neutrino mass matrices of class A are necessarily CP-violating. This feature is, also, apparent in Fig. 2 which depict  $J$  as a function of  $\delta$  for types  $A_1$  [Fig. 2(k)] and  $A_2$  [Fig. 2(l)].

## 4.2 Class B

It can be seen from Table 2 that the mass ratios  $\frac{m_1}{m_2}$  and  $\frac{m_1}{m_3}$  are approximately equal to one for neutrino mass matrices of class B. So, neutrino mass matrices of class B give quasi-degenerate spectrum of neutrino masses. For neutrino mass matrices of class B, the ratio  $\frac{m_1}{m_2}$ , upto first order in  $s_{13}$ , is given by

$$\begin{aligned}
B_1 &: \quad \frac{m_1}{m_2} = 1 + \frac{c_{23}}{c_{12}s_{12}s_{23}^3} s_{13} \cos \delta, \\
B_2 &: \quad \frac{m_1}{m_2} = 1 - \frac{s_{23}}{c_{12}s_{12}c_{23}^3} s_{13} \cos \delta, \\
B_3 &: \quad \frac{m_1}{m_2} = 1 - \frac{c_{23} \tan^2 \theta_{23}}{c_{12}s_{12}s_{23}^3} s_{13} \cos \delta, \\
B_4 &: \quad \frac{m_1}{m_2} = 1 + \frac{s_{23} \cot^2 \theta_{23}}{c_{12}s_{12}c_{23}^3} s_{13} \cos \delta.
\end{aligned} \tag{26}$$

Since, the mass ratio  $\frac{m_1}{m_2}$  is always smaller than one, we find that  $\cos \delta$  should be negative for  $B_1$  and  $B_4$  and positive for  $B_2$  and  $B_3$ , a result that can be gainfully used to distinguish

C.L.	$\alpha$	$M_{ee}$	$J$
1 $\sigma$	$-2.0^0-2.0^0$	$\geq 0.064eV$	$-0.025-0.025$
2 $\sigma$	$-7.7^0-7.7^0$	$\geq 0.037eV$	$-0.036-0.036$
3 $\sigma$	$-22^0-22^0$	$\geq 0.023eV$	$-0.045-0.045$

Table 5: The predictions for neutrino mass matrices of class B.

between mass matrices of class B. Hence,  $B_1$  and  $B_4$  (or  $B_2$  and  $B_3$ ) will have identical predictions for  $\delta$ . Similarly, it can be seen that  $B_1$  and  $B_3$  (or  $B_2$  and  $B_4$ ) will have, almost, identical predictions for  $\theta_{23}$  if it is near maximality. However,  $B_1$  and  $B_4$  (or  $B_2$  and  $B_3$ ) can be distinguished from each other by their predictions for the octant of  $\theta_{23}$  and  $B_1$  and  $B_3$  (or  $B_2$  and  $B_4$ ) can be distinguished from each other by their predictions for the quadrant of  $\delta$ . Thus, the four-fold degeneracy in class B is, now, lifted. Moreover, it follows from Eqs. (26) that the second term should be suppressed by  $s_{13} \cos \delta$  if neutrino mass spectrum is quasi-degenerate ( $m_1 \sim m_2$ ). For large  $\theta_{13}$ , the Dirac phase  $\delta$  should be peaked around  $90^0$  or  $270^0$  to keep the term  $s_{13} \cos \delta$  small. However, for small  $\theta_{13}$ , no additional constraint on  $\delta$  is obtained. The fact that  $\cos \delta$  should be negative for  $B_1$  and  $B_4$  type mass matrices and positive for  $B_2$  and  $B_3$  type mass matrices for the correct sign of  $\Delta m_{12}^2$  results in the elimination of two quadrants of  $\delta$  for each of these subgroups irrespective of the values of the oscillation parameters and their errors. In fact, the earlier analyses [2, 3] do not constrain the Dirac phase  $\delta$  at all for these subgroup of mass matrices. In the analysis by Xing [2], the mass ratios  $\frac{m_1}{m_3}$  and  $\frac{m_2}{m_3}$  were examined and this important constraint on  $\delta$  coming from the mass ratio  $\left(\frac{m_1}{m_2}\right)$  was completely missed as a result. Another detailed numerical analysis by Guo and Xing [3] based upon  $R_\nu$  defined in Eq. (25) does not make use of the solar mass hierarchy as a result of which no constraints on  $\delta$  were obtained for neutrino mass matrices of class B.

Now, we present the numerical results of our analysis for mass matrices of class B. The allowed range of  $\delta$  is  $(90^0 - 270^0)$  for types  $B_1$  and  $B_4$  and  $(-90^0 - 90^0)$  for types  $B_2$  and  $B_3$ . In other words,  $\cos \delta$  is negative for types  $B_1$  and  $B_4$  and positive for types  $B_2$  and  $B_3$ , as expected. This important result is valid irrespective of the ranges of the neutrino oscillation parameters entering in the analysis and is a consequence of the fact that the sign of  $\Delta m_{12}^2$  is positive. If  $\theta_{23} < 45^0$ ,  $B_1$  and  $B_3$  give normal hierarchy while  $B_2$  and  $B_4$  give inverted hierarchy. Similarly, if  $\theta_{23} > 45^0$ , then  $B_1$  and  $B_3$  give inverted hierarchy while  $B_2$  and  $B_4$  give normal hierarchy. Again, this important result is true irrespective of the values of the neutrino oscillation parameters (and their errors) and follows from the dependence of mass ratio  $\left(\frac{m_1}{m_3}\right)$  on  $\tan^2 \theta_{23}$  [Cf. Table 2]. As noted earlier, the four types of neutrino mass matrices within class B differ in their predictions for  $\delta$  and  $\theta_{23}$ . There is no lower bound on  $\theta_{13}$  in class B. The Majorana-type CP-violating phase  $\beta$ , also, remains unconstrained. The predictions for  $\alpha$ ,  $M_{ee}$  and  $J$  for class B mass matrices have been summarized in Table 5. These quantities are the same for mass matrices of types  $B_1$ ,  $B_2$ ,  $B_3$  and  $B_4$ . It can, also, be seen that  $\alpha$  is restricted to a very small range around zero and definite lower bounds on  $M_{ee}$  are obtained. It is important to note that  $\theta_{23} = 45^0$  is disallowed for mass matrices of class B.

In Fig. 3, the correlation plots for all eight possible cases of B type mass matrices ( $B_1$ ,  $B_2$ ,  $B_3$  and  $B_4$  with normal as well as inverted hierarchy) have been shown for  $\alpha$ ,  $\beta$ ,  $\delta$ ,  $\theta_{13}$ ,  $m_1$ ,  $M_{ee}$  and  $J$ . These plots show that B type mass matrices exhibit eightfold degeneracy in the sense that eight different types of mass matrices have identical predictions for these parameters. Figures 3(a-d) depict the correlations of  $\alpha$ ,  $\beta$ ,  $J$  and  $M_{ee}$  with  $\theta_{13}$ . It can be seen from Fig. 3(a) that an upper bound on  $\theta_{13}$  constrains  $\alpha$  to a very narrow range. Even at three standard deviations, the allowed range of  $\alpha$  is  $-22^\circ \leq \alpha \leq 22^\circ$  [Cf. Table 5]. However, no constraints are obtained on the Majorana phase  $\beta$  [Fig. 3(b)]. The correlation plot of  $J$  with  $\theta_{13}$  shows a linear behaviour which is a consequence of  $\theta_{13}$  being small and  $\delta$  being near  $90^\circ$  or  $270^\circ$  for most of the allowed neutrino parameter space. Since,  $M_{ee} \simeq m_1$ , we give the correlation plots for  $M_{ee}$  instead of  $m_1$  in Fig. 3(d) where it can be seen that the absolute neutrino mass scale and 1-3 mixing angles are anti-correlated with each other. Next, we depict the correlations of the quantities  $M_{ee}$  and  $J$  with the Majorana phases  $\alpha$  and  $\beta$  in figures 3(e-h). The effective Majorana mass  $M_{ee}$  diverges at  $\alpha = 0$  and  $\beta = 0$  and so these points are not allowed. A lower bound on  $M_{ee}$  is required to constrain the Majorana phase  $\beta$  which, otherwise, remains unconstrained for mass matrices of class B [Fig. 3(f)]. It can be seen from Fig. 3(g) that  $J$  and  $\alpha$  are directly correlated with each other. This is due to the fact that  $\alpha$  is constrained to a very narrow range around zero degree so that  $\sin \alpha \simeq \alpha$ . The correlation between the two Majorana phases  $\alpha$  and  $\beta$  is depicted in Fig. 3(i) which shows that  $\beta$  will be nearly zero for large  $\alpha$  and vice-versa. Fig. 3(j) depicts the correlation between  $J$  and  $M_{ee}$ . One can see that maximal CP-violation is possible near the lowest possible value of  $M_{ee}$  in class B. It may be worthwhile to mention that the earlier analysis [3] fails to obtain any constraints on the ranges of CP-violating phases ( $\alpha$ ,  $\beta$  and  $\delta$ ) for the reasons discussed earlier.

Fig. 4 depicts the correlations which lift the degeneracy between the neutrino mass matrices of types  $B_1$  ( $B_4$ ) and  $B_2$  ( $B_3$ ). Since, the range of Dirac-type CP-violating phase,  $\delta$ , is different for  $B_1$  ( $B_4$ ) and  $B_2$  ( $B_3$ ), the eightfold degeneracy in B type mass matrices has, now, been reduced to four-fold. The left panel depicts the correlation plots for both  $B_1$  and  $B_4$  and the right panel depicts the correlation plots for  $B_2$  and  $B_3$ . It can be seen from Fig. 4(a,b) that the range of Dirac-type CP-violating phase,  $\delta$ , is  $90^\circ \leq \delta \leq 270^\circ$  ( $-90^\circ \leq \delta \leq 90^\circ$ ) for  $B_1$  and  $B_4$  ( $B_2$  and  $B_3$ ) type mass matrices, as expected. Also, there is a strong correlation between Majorana-type CP violating phase,  $\beta$ , and Dirac-type CP-violating phase,  $\delta$  reinforcing the zeroth order result  $(\beta + \delta = (n + \frac{1}{2})\pi)$  given in Table 2. It can be seen from Fig. 4(c,d) that  $\theta_{13}$  remains unconstrained in all cases because full range of  $\theta_{13}$  is allowed at  $\delta = 90^\circ$  and  $270^\circ$ . However, as we deviate from these values of  $\delta$ ,  $\theta_{13}$  decreases rapidly to very small values. So, if the CP violation is found to be non-maximal,  $\theta_{13}$  will be constrained to very small values. However, if CP violation is found to be nearly maximal,  $\theta_{13}$  can be large. Thus, the suppression factor  $s_{13} \cos \delta$  in the first order correction term in the Taylor expansion for  $(\frac{m_1}{m_2})$  is small as expected from the zeroth order approximation for this class.

Fig. 5 depicts the correlations of  $M_{ee}$  and  $\alpha$  with  $\theta_{23}$ . The correlation plots with  $\theta_{23}$  can be used to further reduce the remaining four-fold degeneracy in B type mass matrices to a two-fold degeneracy which will be lifted by the determination of the neutrino mass hierarchy. The left panel (right panel) depicts the correlation plots for  $B_1(NH)$  and  $B_2(IH)$  ( $B_1(IH)$

	$\beta$	$J$	$M_{ee}$
1 $\sigma$	$-14^0-14^0$	$-0.024-0.024$	$\geq 0.016$ eV
2 $\sigma$	$-16^0-16^0$	$-0.034-0.034$	$\geq 0.013$ eV
3 $\sigma$	$-18^0-18^0$	$-0.045-0.045$	$\geq 0.009$ eV

Table 6: The predictions for  $\beta$ ,  $J$  and  $M_{ee}$  for neutrino mass matrices of class C.

and  $B_2(NH)$ ). The correlation plots of  $M_{ee}$  and  $\alpha$  with  $\theta_{23}$  for  $B_3(NH)$  and  $B_4(IH)$  (or  $B_3(IH)$  and  $B_4(NH)$ ) will be, almost, identical to the plots given in Fig. 5 because  $B_1$  and  $B_3$  (or  $B_2$  and  $B_4$ ) have, almost, identical predictions for  $\theta_{23}$  and, therefore, are not given here. It can be seen from Fig. 5(a,b) that the effective Majorana mass  $M_{ee}$  is strongly correlated with  $\theta_{23}$ . Moreover, maximal value of  $\theta_{23}$  is not allowed by the current neutrino oscillation data since  $M_{ee}$  diverges at  $\theta_{23} = \frac{\pi}{4}$ . Larger the deviation of  $\theta_{23}$  from maximality, smaller is the value of  $M_{ee}$ . Also, a large value of  $\alpha$  implies large deviations of  $\theta_{23}$  from maximality. The extent of the deviation of 2-3 mixing from maximality is governed by the magnitude of the upper bound on  $M_{ee}$  while the direction of the deviation from maximality is governed by the quadrant of  $\delta$  and the neutrino mass hierarchy.

### 4.3 Class C

It can be seen from Table 2 that the mass ratio  $\frac{m_1}{m_2}$  is greater than one at zeroth order. However, the higher order terms in the Taylor series expansion of the ratio  $\frac{m_1}{m_2}$  may make it smaller than one. Detailed numerical analysis shows that this actually happens and the mass matrices of class C are marginally allowed. The Taylor series expansion for  $\frac{m_1}{m_2}$  to first order in  $s_{13}$  is given by

$$\frac{m_1}{m_2} = \frac{1}{\tan^2 \theta_{12}} \left( 1 - \frac{\tan 2\theta_{23}}{s_{12}c_{12}} s_{13} \cos \delta \right). \quad (27)$$

For  $\frac{m_1}{m_2}$  to be smaller than one, the term  $(\tan 2\theta_{23} \cos \delta)$  should be positive. Therefore, when  $\theta_{23} < 45^0$ , we must have  $-90^0 < \delta < 90^0$ . Similarly, when  $\theta_{23} > 45^0$ , we must have  $90^0 < \delta < 270^0$ . Just like class B, the correlation between the octant of  $\theta_{23}$  and the quadrant of  $\delta$  obtained here for class C is independent of the ranges of the neutrino oscillation parameters and is a generic feature of two texture zero mass matrices. The points  $\delta = 90^0, 270^0$  and  $\theta_{13} = 0^0$  are not allowed because the first order correction term vanishes at these points. The mixing angle  $\theta_{23}$  should approach  $45^0$  as  $\delta$  approaches  $90^0$  or  $270^0$  and  $\theta_{13}$  approaches  $0^0$  so that the term  $(s_{13} \tan 2\theta_{23} \cos \delta)$  can make the ratio  $\frac{m_1}{m_2}$  smaller than one. The mass ratio  $\frac{m_1}{m_3}$  is greater than one at the zeroth order. Therefore, neutrino mass matrices of type C may be expected to be consistent with inverted hierarchy only. However, we shall see in the detailed numerical analysis that the normal hierarchy is, also, allowed marginally.

For mass matrices of type C, with inverted hierarchy, the allowed ranges for the parameters  $\beta$ ,  $J$  and  $M_{ee}$  are given in Table 6. All other parameters remain unconstrained. The correlation

plots between various parameters have been depicted in Figs. 6-8. In Fig. 6, we have given the correlations of  $\alpha$ ,  $\beta$ ,  $\theta_{13}$ ,  $\theta_{23}$ ,  $M_{ee}$  and  $J$  with  $\delta$ . As discussed earlier, the values  $\delta = 90^\circ$  and  $270^\circ$  are not allowed [Fig. 6(a)]. Therefore, maximal CP-violation is not allowed for mass matrices of class C. For the maximal values of  $\delta$ ,  $\alpha$  should be equal to zero. Therefore, the point  $\alpha = 0^\circ$  is, also, not allowed. However, all other values of  $\alpha$  are allowed. It can be seen from Fig. 6(b) that the Majorana phase  $\beta$  is a periodic function of  $\delta$  with a period of  $180^\circ$  and  $\beta$  can be zero at  $\delta = 0^\circ$  or  $180^\circ$ . However, the points  $(\beta = 0^\circ, \delta = 90^\circ)$  and  $(\beta = 0^\circ, \delta = 270^\circ)$  are disallowed. The correlation between  $\delta$  and  $\theta_{13}$  has been depicted in Fig. 6(c). The correlation between  $\delta$  and  $\theta_{23}$  has been depicted in Fig. 6(d) where it can be seen that the maximal 2-3 mixing is not allowed. However, the mixing angle  $\theta_{23}$  will be below maximality if  $\cos \delta$  is positive ( $-90^\circ$ - $90^\circ$ ) and above maximality if  $\cos \delta$  is negative ( $90^\circ$ - $270^\circ$ ). These conclusions are, completely, in agreement with the results obtained from the Taylor series expansion. Fig. 6(e) depicts the correlation between  $M_{ee}$  and  $\delta$  which yields a lower bound of about 0.02 eV on  $M_{ee}$  for  $\delta = 0^\circ$  or  $180^\circ$  for neutrino mass matrices of class C. As  $\delta$  deviates from the values  $0^\circ$  and  $180^\circ$ ,  $M_{ee}$  increases and diverges as  $\delta$  becomes maximal. The correlation between  $J$  and  $\delta$  has been shown in Fig. 6(f).

In Fig. 7, we have shown the correlations of  $\alpha$ ,  $\beta$ ,  $\theta_{23}$  and  $J$  with  $\theta_{13}$ . In Fig. 7(a),  $(\theta_{13}, \alpha)$  correlation has been depicted. Full range ( $-90^\circ$ - $90^\circ$ ) for  $\alpha$  is allowed for  $\theta_{13} = 0$ . However, it can be seen from Fig. 7(a) that a lower bound on  $\theta_{13}$  of about  $4^\circ$  will constrain  $\alpha$  to the range ( $-65^\circ$ - $65^\circ$ ). As noted earlier,  $\beta$  is, already, constrained to a small range around zero. However, it can be seen from Fig. 7(b) that  $\beta$  can be further constrained if  $\theta_{13}$  is found to be larger than  $3^\circ$ . A lower bound on  $\theta_{13}$  larger than  $3^\circ$  will disallow a finite range of  $\beta$  around zero. From the  $(\theta_{13}, \theta_{23})$  correlation plot [Fig. 7(c)], it can be seen that larger the value of  $\theta_{13}$ , larger will be the deviation of  $\theta_{23}$  from maximality. The point  $(\theta_{13} = 0^\circ, \theta_{23} = 45^\circ)$  is not allowed. The disallowed range of  $\theta_{23}$  around  $45^\circ$  increases with increase in  $\theta_{13}$ . For example, the disallowed range of  $\theta_{23}$  at  $\theta_{13} = 6^\circ$  is approximately  $44^\circ - 46^\circ$ . For small values of  $\theta_{13}$ ,  $J$  is proportional to  $\theta_{13}$  and the constant of proportionality is determined by  $\sin \delta$  [Cf. Eq. (23)]. These features can be seen graphically in the correlation plot between  $J$  and  $\theta_{13}$  depicted in Fig. 7(d).

Some other important correlation plots have been shown in Fig. 8. It can be seen from the  $(\alpha, \beta)$  correlation plot [Fig. 8(a)] that the two Majorana phases can not vanish simultaneously. The correlation between  $M_{ee}$  and  $\alpha$  has been shown in Fig. 8(c) where it can be seen that an upper bound on  $M_{ee}$  will reject a considerable range of  $\alpha$ . The  $(M_{ee}, \beta)$  correlation plot has been given in Fig. 8(d). It can be seen that the allowed range of  $\beta$  (which is  $-15^\circ$ - $15^\circ$  for small values of  $M_{ee}$ ) can be further constrained if  $M_{ee}$  is found to be larger than 0.03 eV. Fig. 8(e) depicts the correlation between  $M_{ee}$  and  $\theta_{23}$ . It can be seen that  $M_{ee}$  diverges for maximal 2-3 mixing. A lower bound on  $M_{ee}$  can be used to constrain  $\theta_{23}$ .

For  $C$  type mass matrices, with normal hierarchy Dirac-type CP-violation phase,  $\delta$ , can have only two values  $\delta = 90^\circ$  or  $180^\circ$ . Majorana-type CP-violating phases ( $\alpha$  and  $\beta$ ) and  $\theta_{13}$  remain unconstrained. There is a strong correlation between  $\theta_{13}$  and  $\theta_{23}$  in this case. Larger the allowed range of  $\theta_{13}$ , larger will be the deviation of  $\theta_{23}$  from maximality. The neutrino mass matrices of class C were examined analytically in [10] where some of the results reported here for class C have been obtained.

## 4.4 Eightfold degeneracy

The forthcoming neutrino experiments will aim at measuring the neutrino mass hierarchy, Dirac type CP violating phase  $\delta$  and the deviations of the atmospheric mixing angle from maximality [19]. The results of these experiments will fall in one of the following eight categories of phenomenological interest:

1. NH,  $\theta_{23} < 45^\circ$  and  $90^\circ < \delta < 270^\circ$ ,
2. NH,  $\theta_{23} > 45^\circ$  and  $-90^\circ < \delta < 90^\circ$ ,
3. NH,  $\theta_{23} < 45^\circ$  and  $-90^\circ < \delta < 90^\circ$ ,
4. NH,  $\theta_{23} > 45^\circ$  and  $90^\circ < \delta < 270^\circ$ ,
5. IH,  $\theta_{23} > 45^\circ$  and  $90^\circ < \delta < 270^\circ$ ,
6. IH,  $\theta_{23} < 45^\circ$  and  $-90^\circ < \delta < 90^\circ$ ,
7. IH,  $\theta_{23} > 45^\circ$  and  $-90^\circ < \delta < 90^\circ$ ,
8. IH,  $\theta_{23} < 45^\circ$  and  $90^\circ < \delta < 270^\circ$ .

The eight cases given above are degenerate for the present neutrino oscillation data because of the octant degeneracy of  $\theta_{23}$  (i.e. if  $\theta_{23} < 45^\circ$  or  $\theta_{23} > 45^\circ$ ), the intrinsic degeneracy in the sign of  $\cos \delta$  and the two-fold degeneracy in the sign of  $\Delta m_{23}^2$ . This degeneracy known as the eightfold degeneracy in the neutrino parameter space has been studied extensively in the literature [19, 20, 21, 22]. A specific project named Tokai-to-Kamioka-Korea (T2KK) two detector complex which will receive neutrino superbeams from J-PARC has been proposed [22] to resolve these degeneracies. The intrinsic degeneracy in the sign of  $\cos \delta$  will be resolved by the spectrum information at T2KK and the degeneracy in the sign of  $\Delta m_{23}^2$  will be resolved by observing the difference in the earth matter effects between the intermediate and far detectors. The  $\theta_{23}$  octant degeneracy will be resolved by observing the difference in  $\Delta m_{12}^2$  oscillation effects between the intermediate and far detectors at T2KK. In addition, neutrino factories [23] and beta-beam experiments [24] have the potential to resolve the eightfold degeneracy.

## 5 Conclusions

If neutrinoless double beta decay searches give positive results and  $M_{ee}$  is measured experimentally or the atmospheric/reactor neutrino oscillation experiments confirm inverted hierarchy, the neutrino mass matrices of class A will be ruled out. A generic prediction of this class of models is a lower bound on  $\theta_{13}$  [Table 3]. If the forthcoming neutrino oscillation experiments measure  $\theta_{13}$  below  $3.3^\circ$ , the neutrino mass matrices of class A will, again, be ruled out. If  $M_{ee}$  is found to be non-zero, the mass matrices of class B or C may be allowed. The eight different types of mass matrices in class B can be distinguished from one another

Categories	Degeneracies			Matrices		
	sign of $\Delta m_{23}^2$	sign of $\cos 2\theta_{23}$	sign of $\cos \delta$	$A$	$B$	$C$
1	+	+	−	$A_2$	$B_1(NH)$	×
2	+	−	+	$A_1$	$B_2(NH)$	×
3	+	+	+	×	$B_3(NH)$	×
4	+	−	−	×	$B_4(NH)$	×
5	−	−	−	×	$B_1(IH)$	×
6	−	+	+	×	$B_2(IH)$	$C(IH)$
7	−	−	+	×	$B_3(IH)$	$C(IH)$
8	−	+	−	×	$B_4(IH)$	×

Table 7: The consequences of resolving the eightfold experimental degeneracies for the neutrino mass matrices with two texture zeros.

by the future experiential data by the resolution of the eightfold degeneracy of the neutrino parameter space. The observation of correlations between various neutrino parameters like  $\theta_{13}$ ,  $\theta_{23}$ ,  $\delta$  and  $M_{ee}$  etc. will confirm the neutrino mass matrices with two texture zeros. Moreover, the CP-violation in lepton number conserving and non-conserving processes will be correlated in a definite way and there will be only one independent CP-violating measure for both types of processes.

Main conclusions of the present study have been summarized in Table 7 which shows how the resolution of the degeneracies of neutrino parameter space will resolve the degeneracies of the neutrino mass matrices. As an illustration for the use of Table 7, we look at the results obtained for category 1 for which the signs of  $\Delta m_{23}^2$  and  $\cos \theta_{23}$  are positive and the sign of  $\cos \delta$  is negative. For this category, the neutrino mass matrices of type  $A_2$  and  $B_1$  (for normal hierarchy only) may explain the neutrino data whereas the mass matrices of class C are ruled out. Other possibilities summarized in Table 7 may be understood similarly. It is found that the degeneracies in the neutrino parameter space are inextricably linked to the degeneracies in the neutrino mass matrix and by finding the hierarchy, octant of  $\theta_{23}$  and sign of  $\cos \delta$ , the future experiments will settle the fate of neutrino mass matrices with two texture zeros. The resolution of the eightfold degeneracy in the neutrino parameter space will, also, resolve the eightfold degeneracy of the neutrino mass matrices of class B as can be seen from figures 4 and 5. Figures 4 and 5, also, illustrate the decoupling of degeneracies in the sense that two mass matrices can be degenerate in their  $\delta$  predictions but may have different predictions for  $\theta_{23}$  or vice-versa. A similar decoupling of degeneracies occur in neutrino oscillation experiments with matter effects [21] where an experiment may be insensitive to the sign of  $\cos \delta$  but can resolve the degeneracy in the sign of  $\cos 2\theta_{23}$  or it can be insensitive to the sign of  $\cos 2\theta_{23}$  but can resolve the degeneracy in the sign of  $\cos \delta$ .

## 6 Acknowledgments

The research work of S. D. and S. V. is supported by the Board of Research in Nuclear Sciences (BRNS), Department of Atomic Energy, Government of India *vide* Grant No. 2004/37/23/BRNS/399. S. K. acknowledges the financial support provided by Council for Scientific and Industrial Research (CSIR), Government of India. We would like to thank Manmohan Gupta for critical reading of the manuscript and helpful suggestions.

## References

- [1] Paul H. Frampton, Sheldon L. Glashow and Danny Marfatia, *Phys. Lett.* **B 536**, 79 (2002); Bipin R. Desai, D. P. Roy and Alexander R. Vaucher, *Mod. Phys. Lett.* **A 18**, 1355 (2003).
- [2] Zhi-zhong Xing, *Phys. Lett.* **B 530** 159 (2002).
- [3] Wanlei Guo and Zhi-zhong Xing, *Phys. Rev.* **D 67**, 053002 (2003).
- [4] Alexander Merle and Werner Rodejohann, *Phys. Rev.* **D 73**, 073012 (2006); S. Dev and Sanjeev Kumar, hep-ph/0607048.
- [5] S. Dev, Sanjeev Kumar, Surender Verma and Shivani Gupta, hep-ph/0611313.
- [6] G. C. Branco, R. Gonzalez Felipe, F. R. Joaquim and T. Yanagida, *Phys. Lett.* **B 562** 265 (2003); Bhag C. Chauhan, Joao Pulido and Marco Picariello, *Phys. Rev.* **D 73**, 053003 (2006).
- [7] Xiao-Gang He and A. Zee, hep-ph/0302201 v2.
- [8] Suraj. N. Gupta and Subhash Rajpoot, “Quark Mass Matrices and the Top Quark Mass”, Wayne State University Preprint, September 1990; S. N. Gupta and J. M. Johnson, *Phys. Rev.* **D 44**, 2110 (1991); S. Rajpoot, *Mod. Phys. Lett.* **A 7**, 309 (1992); H. Fritzsch and Z.Z. Xing, *Phys. Lett.* **B 353**, 114 (1995).
- [9] P. H. Frampton, M. C. Oh and T. Yoshikawa, *Phys. Rev.* **D 66**, 033007 (2002).
- [10] Walter Grimus and Luis Lavoura, *J. Phys.* **G 31**, 693-702 (2005).
- [11] H. C. Goh, R. N. Mohapatra and Siew-Phang Ng, *Phys. Rev.* **D 68**, 115008 (2003).
- [12] S. Kaneko, M. Katsumata and M. Tanimoto, *JHEP* **0307**, 025 (2003).
- [13] G. L. Fogli *et al*, hep-ph/0506083 v1.
- [14] M. Maltony, T. Schwetz, M. A. Tortola and J. W. F. Valle, hep-ph/0405172 v5.
- [15] J. Nelson, Talk at Neutrino 2006, 1319 June 2006, Santa Fe, New Mexico, <http://neutrinosantafe06.com>.



- [16] B. Aharmim *et al.* [SNO collaboration], *Phys. Rev. C* **72**, 055502 (2005), nucl-ex/0502021.
- [17] T. Araki et al. [KamLAND Collaboration], hep-ex/0406035; Talk by G. Gratta at Neutrino 2004, 1419 June 2004, Paris, <http://neutrino2004.in2p3.fr>.
- [18] C. Jarlskog *Phys. Rev. Lett.* **55**, 1039 (1985).
- [19] E. Abouzaid *et al.*, Report of the APS Neutrino Study Reactor Working Group, 2004.
- [20] Hisakazu Minakata, Hiroshi Nunokawa, Stephen Parke, *Phys. Rev. D* **66**, 093012 (2002).
- [21] Takaaki Kajita, Hisakazu Minakata, Shoei Nakayama, and Hiroshi Nunokawa, *Phys. Rev. D* **75**, 013006 (2007).
- [22] Hisakazu Minakata, hep-ph/0701070.
- [23] Raj Gandhi and Walter Winter, hep-ph/0612158; A. M. Gago and J. Jones Perez, hep-ph/0611110.
- [24] E. Fernandez-Martinez, hep-ph/0605101; A. Donini and E. Fernandez-Martinez, *Phys. Lett. B* **641** 432(2006), hep-ph/0603261.

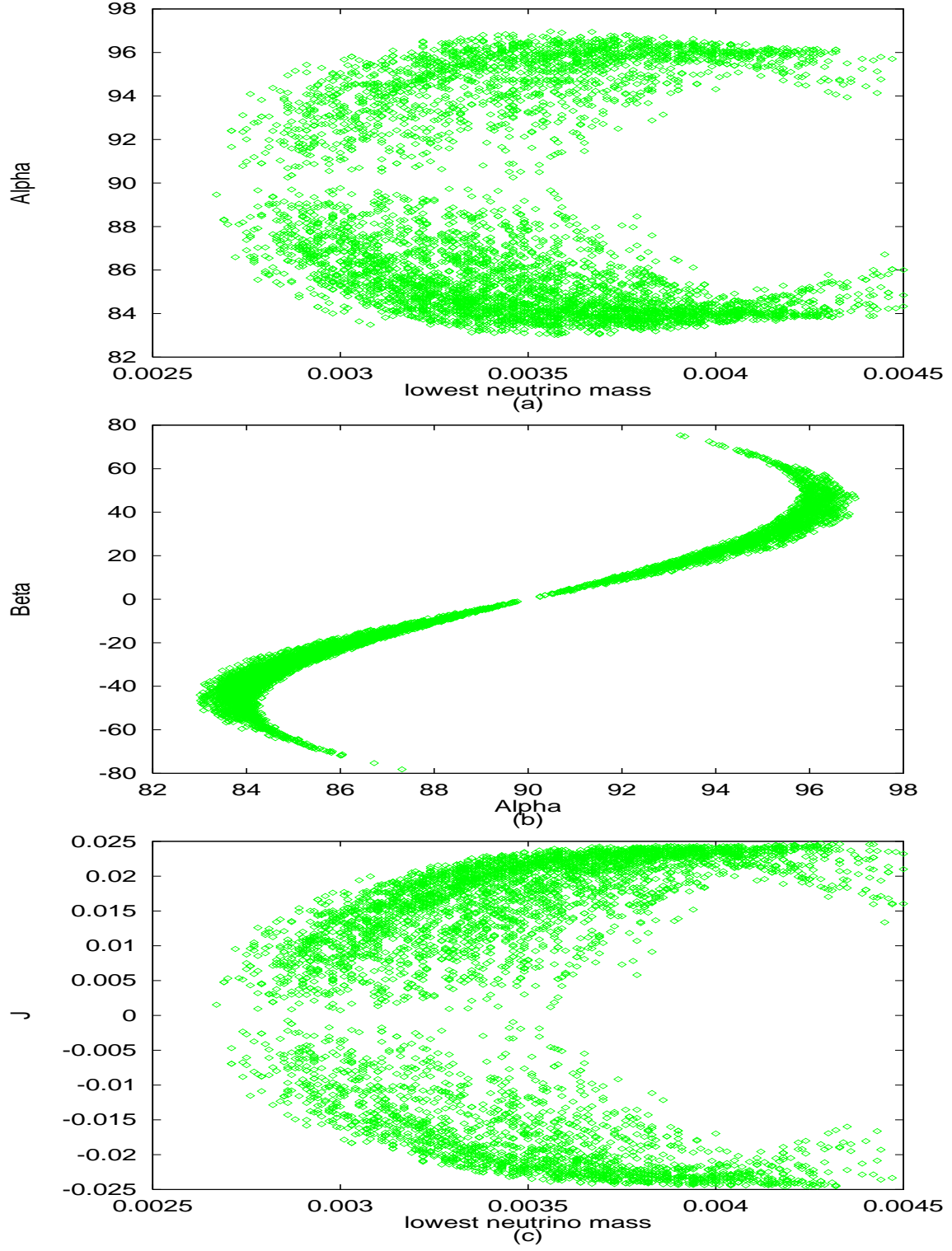


Figure 1: Correlation plots for neutrino mass matrices of class A at one standard deviation.

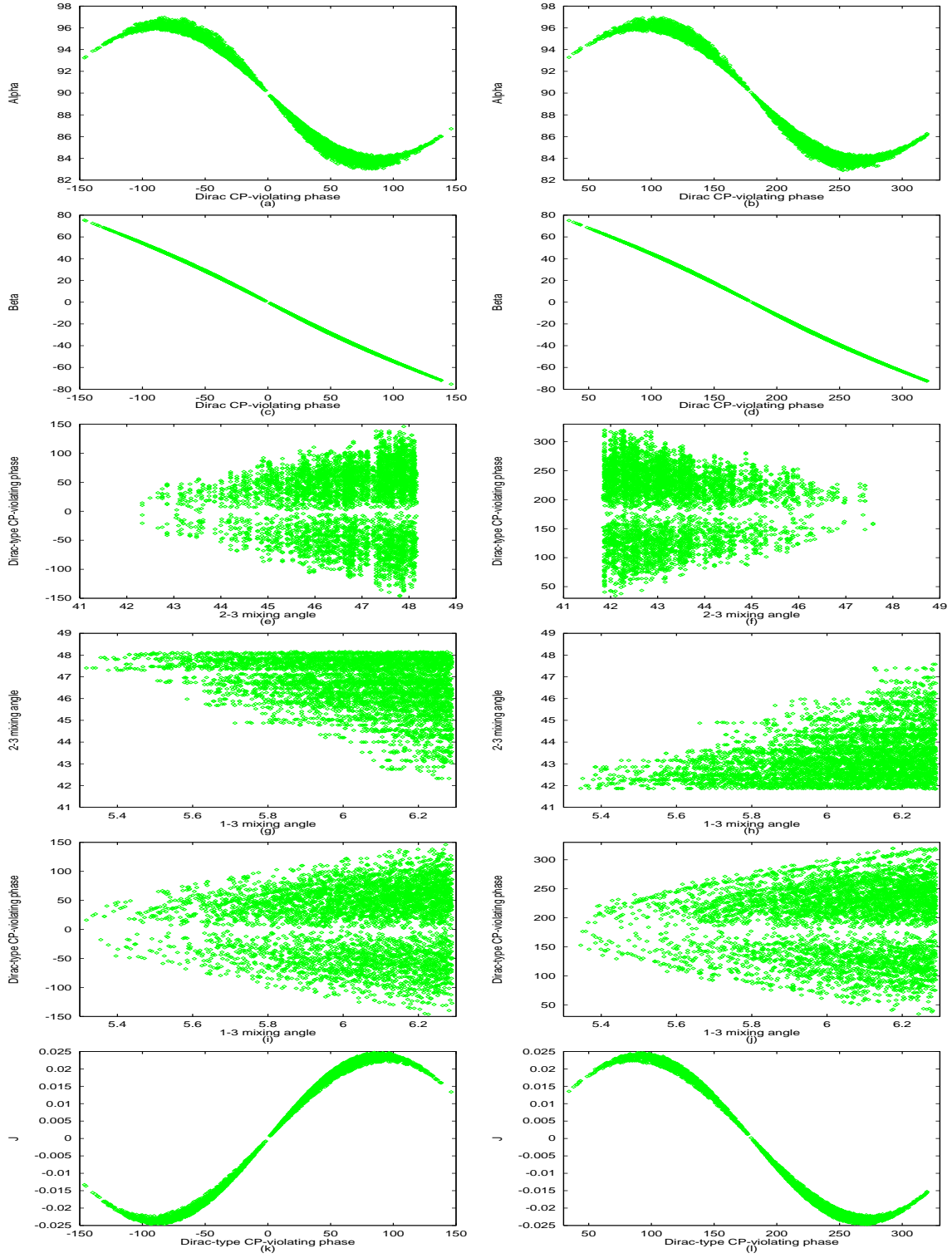


Figure 2: Correlation plots for neutrino mass matrices of type  $A_1$  (left panel) and  $A_2$  (right panel).

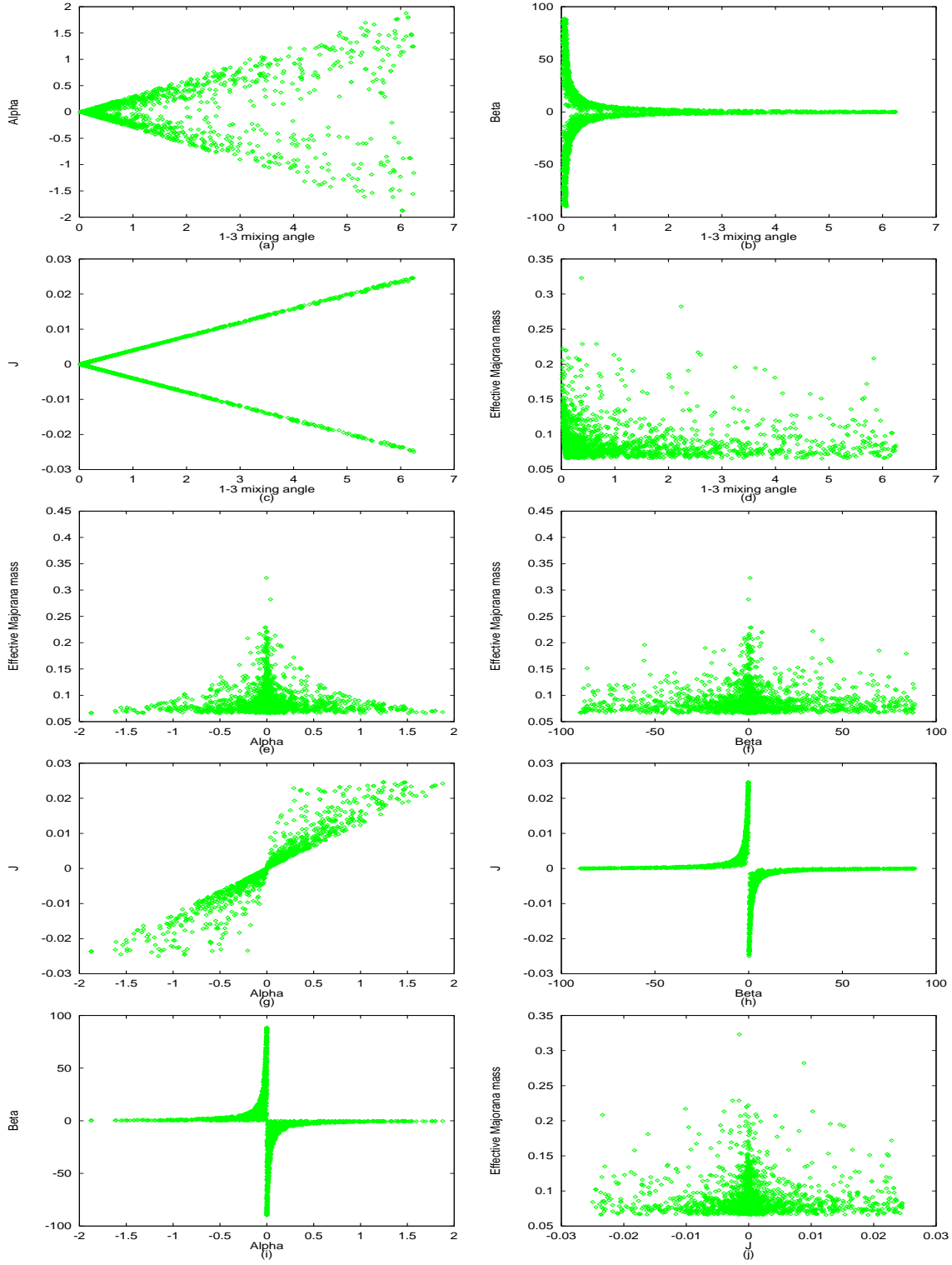


Figure 3:  $1\sigma$  correlation plots for  $B_1$ ,  $B_2$ ,  $B_3$  and  $B_4$  type mass matrices with normal as well as inverted hierarchies.

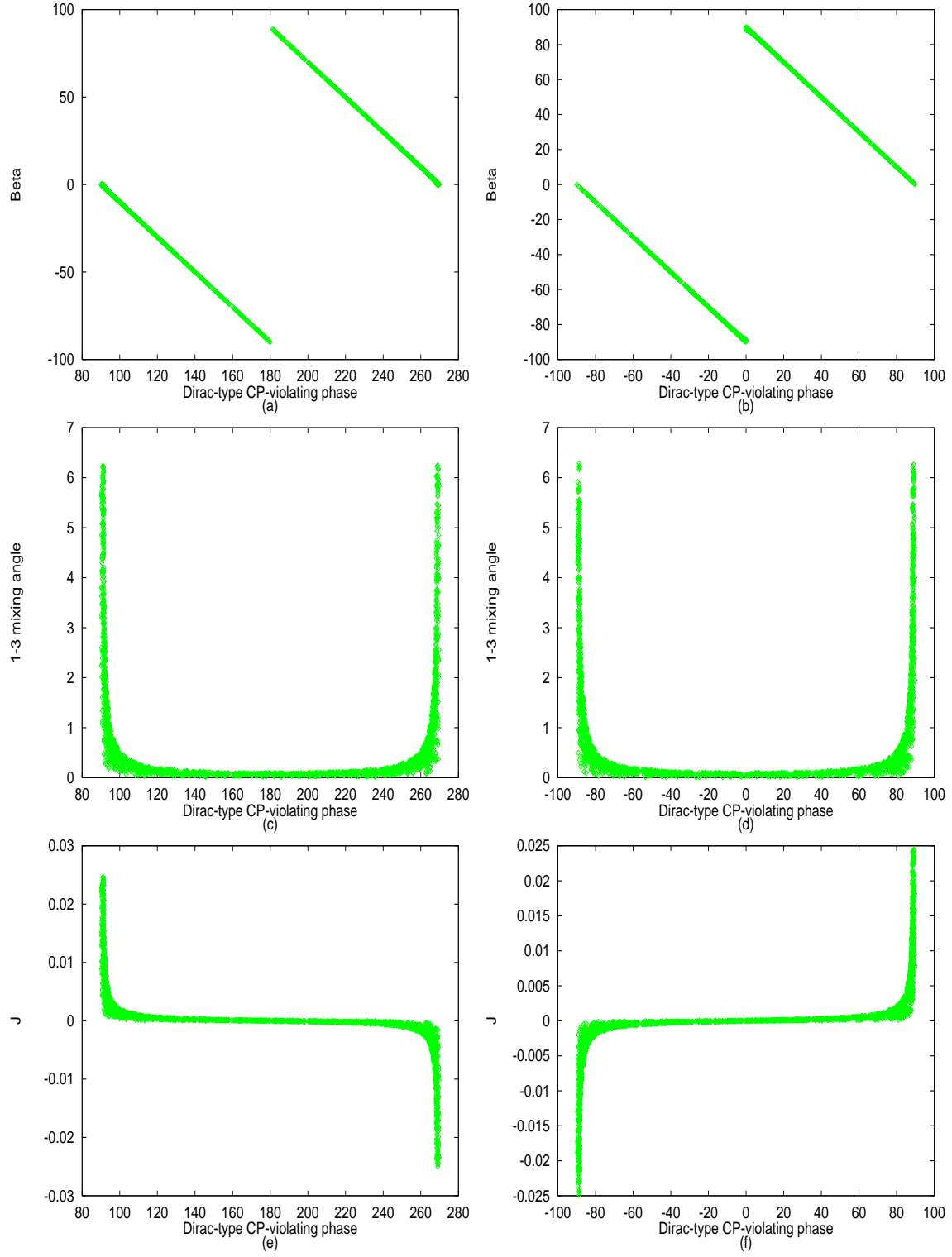


Figure 4: The left panel shows the correlation plots for  $B_1$  or  $B_4$  while right panel shows the correlation plots for  $B_2$  or  $B_3$  type mass matrices.

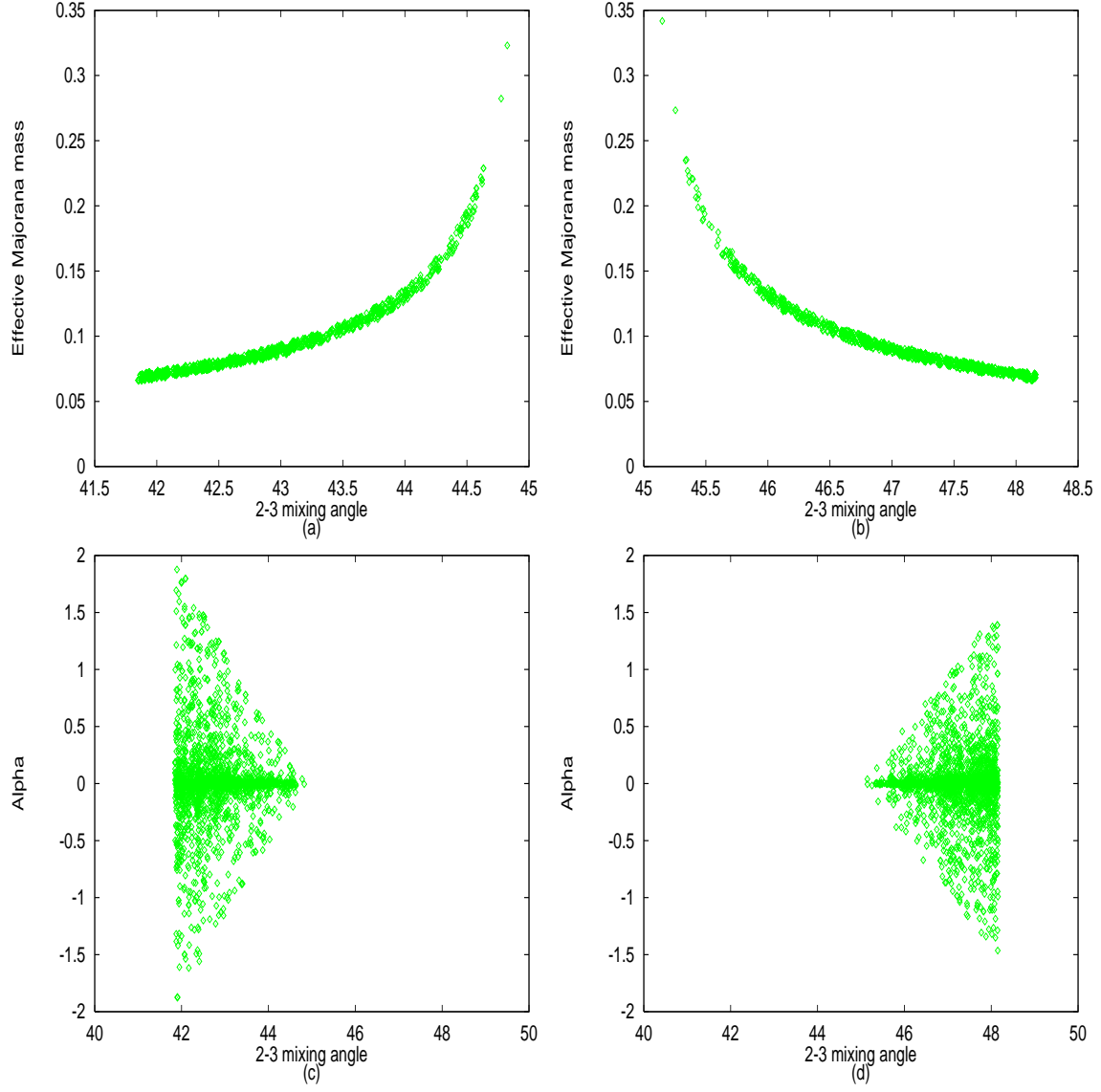


Figure 5: Variation of  $M_{ee}$  and  $\alpha$  with  $\theta_{23}$ . The left [right] panel plots are for  $B_1(NH)$ ,  $B_2(IH)$  [  $B_3(IH)$ ,  $B_4(NH)$  ] type mass matrices.

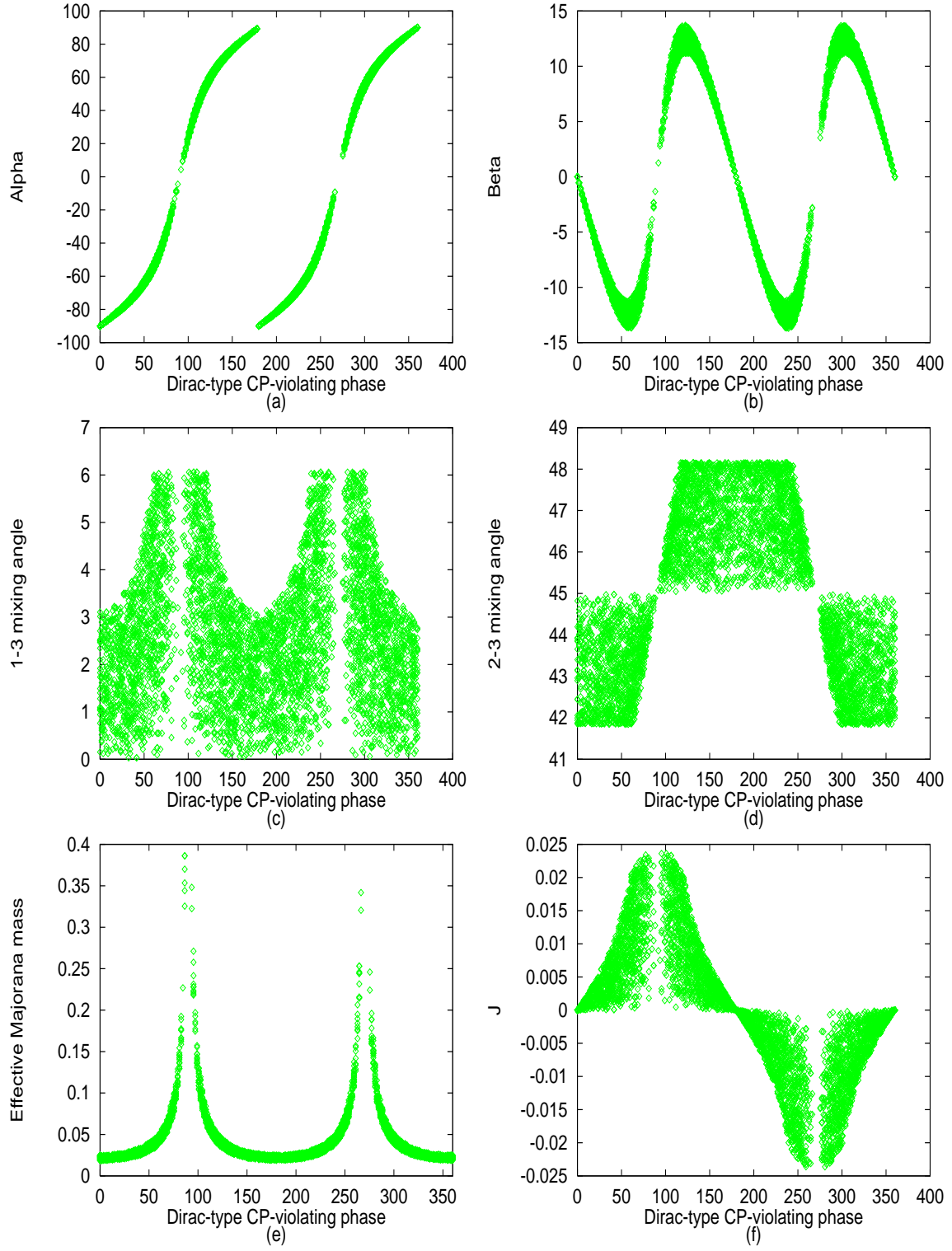


Figure 6: The correlation plots for CP-violating phase  $\delta$  for neutrino mass matrices of type C with inverted hierarchy.

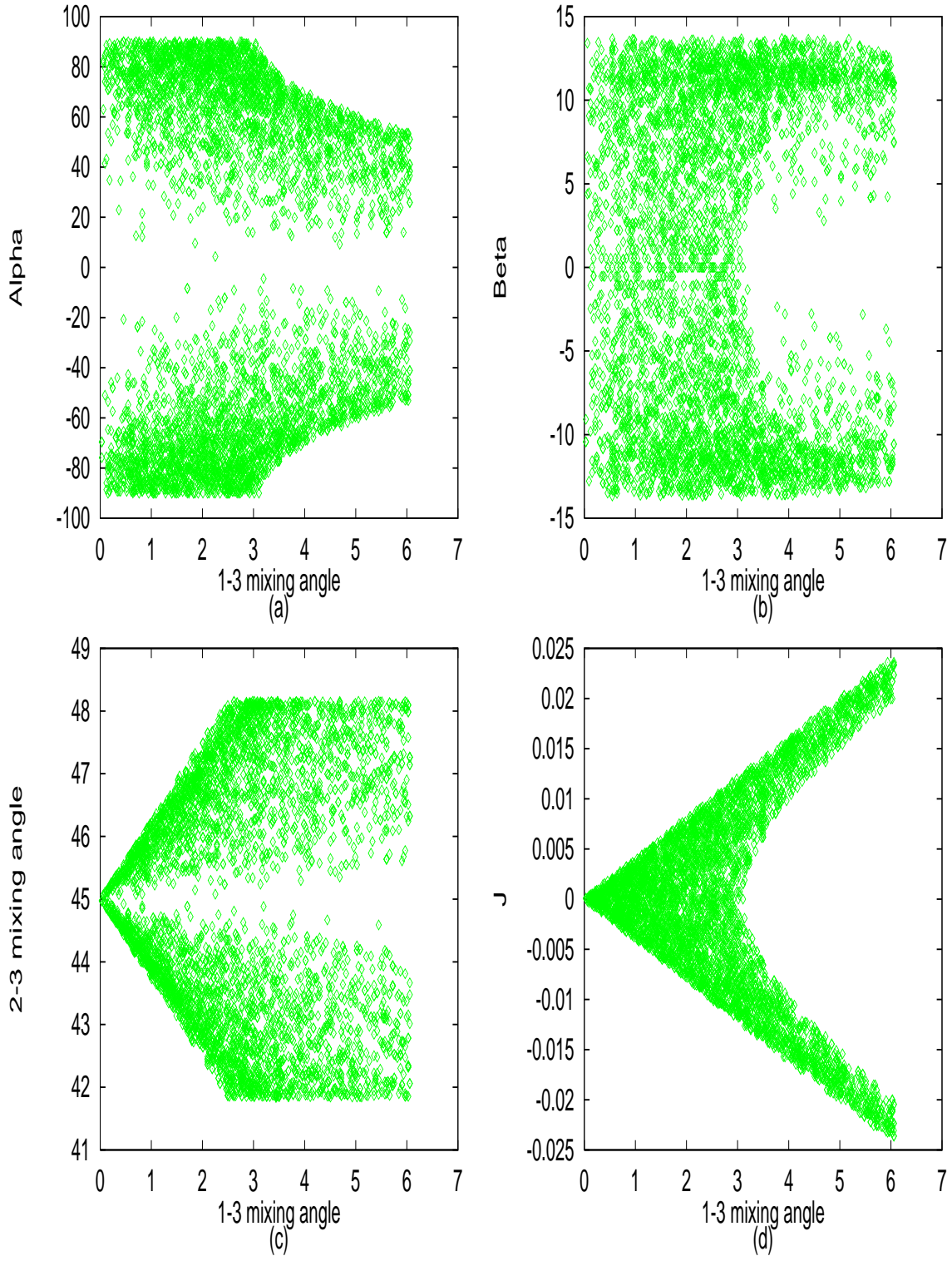


Figure 7: The correlation plots for the mixing angle  $\theta_{13}$  for neutrino mass matrices of type C with inverted hierarchy.



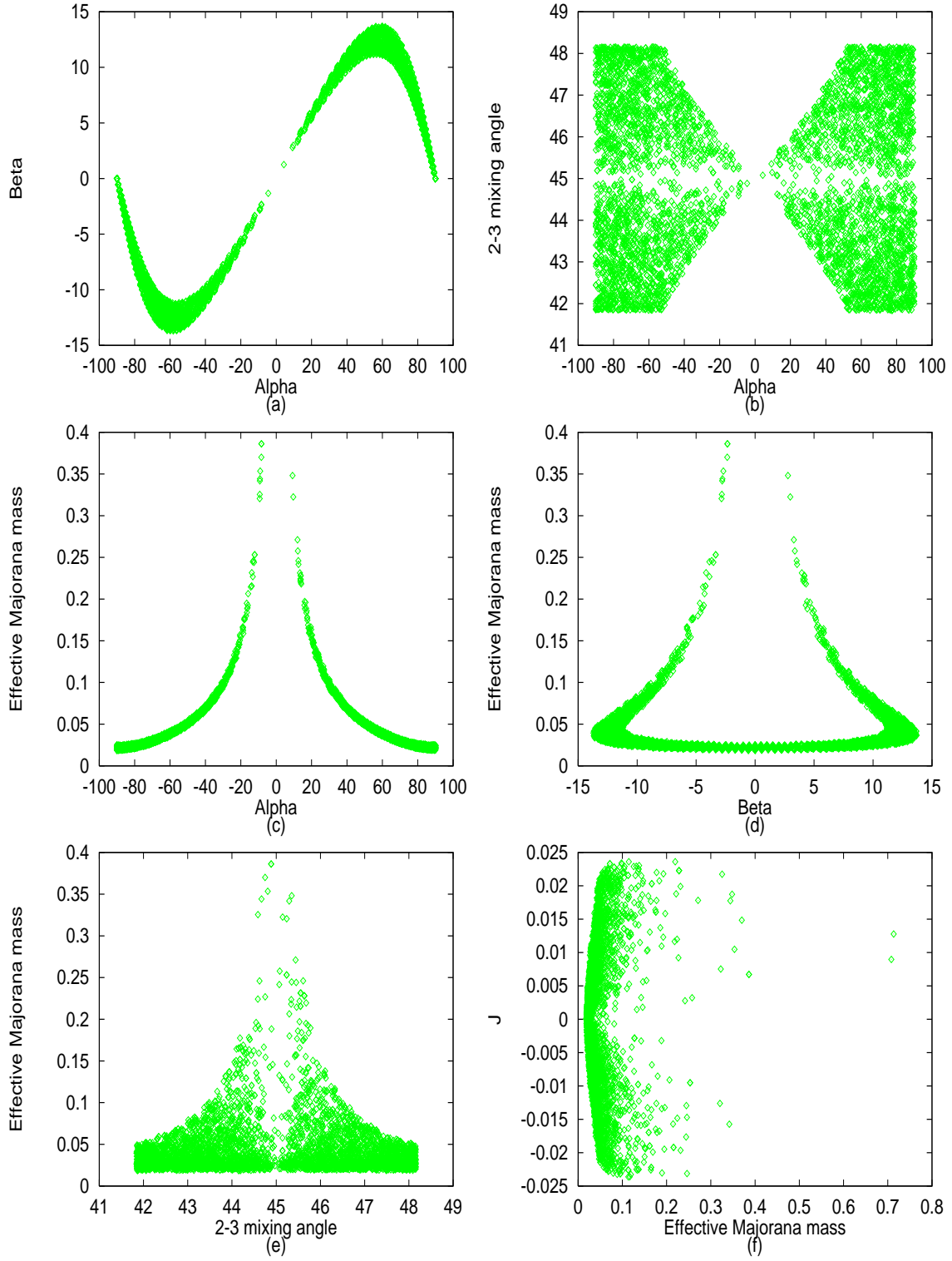


Figure 8: Some other important correlation plots for neutrino mass matrices of type C with inverted hierarchy.